A dynamic model of complexly mechanoresponsive chain-poly[n]-catenations in double-network polyampholyte hydrogels

Ziyu Xing[1], Haibao Lu[1,*] and Yong Qing Fu[2]

[1]National Key Laboratory of Science and Technology on Advanced Composites in Special Environments, Harbin Institute of Technology, Harbin 150080, China

[2]Faculty of Engineering and Environment, University of Northumbria, Newcastle upon Tyne, NE1 8ST, UK

[*]Corresponding author, E-mail: luhb@hit.edu.cn

Abstract: Polyampholytes have been widely used to improve mechanical performance of double-network (DN) hydrogels, however, their complex mechanisms of electric charge reactions and chain catenations have not been well understood. In this study, a collective and cooperative model is developed to describe the dynamics and constitutive relationships of complexly mechanoresponsive chain-poly[n]-catenations in polyampholyte DN hydrogels. The freely jointed chain (FJC) model and Flory-Huggins theory are firstly employed to formulate mechanochemical behaviors of the DN hydrogels, in which the stretchable network undergoes a folding-to-unfolding transition and the brittle one undergoes a reversibly mechanochemical transition. The worm like chain (WLC) model is then introduced to describe the chain-poly[n]-catenations, of which the strong and weak ionic bonds have been modeled based on the entanglement and dangling effects, respectively. Finally, a free-energy equation is developed to describe their collective and cooperative dynamics. Effectiveness of the newly proposed model is verified by

applying it to predict the experimental results of the polyampholyte DN hydrogels reported in literature.

Keywords: Polyampholyte; double-network hydrogel; dynamic model; catenations

1. Introduction

Hydrogel is one of the most popular responsive materials with capabilities of large and reversible deformations [1-3]. In terms of their thermodynamics of polymer solutions, hydrogels are normally regarded as rubbery-like soft matters, and thus respond to the external stress in an elastic manner [5-8]. Therefore, thermomechanical behaviors of the hydrogels have been generally described using the rubber elasticity theory and Flory-Huggins solution theory [9-14]. Significant progress has recently also been made to reproduce their constitutive relationships using free energy functions [16-20].

However, hydrogels normally show low stiffness and strength [4], thus double networks (DN) hydrogels have been developed to improve their mechanical performance [6-13]. These DN hydrogels are incorporated of two distinctive types of polymeric network components, which are referred to the first brittle networks and the second ductile ones [14,15]. The presence of first brittle networks helps to resist the mechanical loading by means of mechanochemical kinetics of sacrificial covalent bonds [6-13]. The enhanced strength has been attributed to the fracture of these brittle networks, which are helpful to enhance both the elastic modulus and true stress of break [21,22]. Owing to the oppositely mechanical responses of these two networks,

the DN hydrogel generally undergoes a cooperative and complex thermodynamics in response to an externally mechanical loading [23-26].

Several other types of DN hydrogels have further been developed to improve the mechanical strength and toughness, e.g., replacing the covalent bonds (which have poor reversibility), using ionic bonds [27-30] or hydrogen bonds [31], and adding monomers in solvents [32,33]. It has been reported that polyampholyte DN hydrogel has a classical entanglement effect in its macromolecule chains due to the charge attractions of ionic bonds, thus enhancing the mechanical properties of the DN hydrogels [27,28]. However, due to their complex thermodynamics, few theoretical models have been developed to explore the toughening mechanisms of these polyampholyte DN hydrogels which show extremely high mechanical strengths [34].

In this study, a collective and cooperative model is developed to describe the dynamics of mechanoresponsive chain-poly[n]-catenations and the constitutive relationships of polyampholyte DN hydrogels. The folding-to-unfolding transition of stretchable network [35-40], the reversibly mechanochemical transition of sacrificially brittle network and entanglement effect of polyampholyte macromolecule chains have been formulated using the freely jointed chain (FJC) model, Flory-Huggins theory and worm like chain (WLC) model [35-37], respectively. The chain-poly[n]-catenations, including folding-to-unfolding transition, mechanochemical transition, entanglement of strong ionic bonding and dangling effect of weak ionic bonds, have been identified as the driving forces for polyampholyte DN hydrogels with extremely high mechanical strength. Finally, the

analytical results obtained using the newly proposed models are verified using the experimental data reported in literature.

2. Theoretical framework of DN hydrogel

2.1 Folding-to-unfolding transition of stretchable network

In the DN hydrogel, the brittle and stretchable networks undergo different mechanical deformation simultaneously, as revealed in Figure 1(a). Therefore, it is necessary to model the different mechanical behaviors of these two types of networks. The stretchable network generally shows a linearly elastic behavior. Therefore, the freely jointed chain (FJC) model [41-43] can be used to characterize the folding-to-unfolding transition of stretchable network. In Figure 1(b), the FJC model, freely rotating chain (FRC) model and worm like chain (WLC) model [35-37] have been illustrated for comparisons. In this figure, l_b is the length of the rotating unit, and l_p is the persistence length. l_k is the length of Kuhn segment.

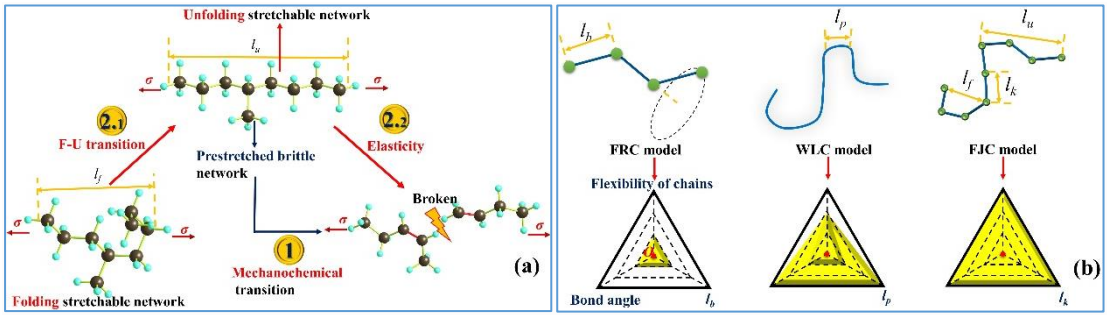

Figure 1. (a) Illustration of the folding-to-unfolding transition in DN hydrogels. (b) Illustration of flexibility of macromolecule chain using the FRC, WLC and FJC models.

These statistical rubber elastic models, including WLC model [44] and FJC model [45], have been investigated extensively and verified experimentally [44-47]. They

can provide the foundations for the establishment of hydrogel models. All these three models can explain the distribution and flexibility of macromolecule chains within the DN hydrogels. However, the FJC model is helpful to characterize the stretchable folding-to-unfolding behavior. Based on the previous studies [41-43], conformation number of the FJC model (Ω_{FJ}) can be written as,

$$\Omega_{FJ} = k_{FJ} \exp\left[-\frac{h_{FJ}}{l_k} L^{-1}\left(\frac{h_{FJ}}{Nl_k}\right) - N \ln \frac{L^{-1}\left(\frac{h_{FJ}}{Nl_k}\right)}{\sinh L^{-1}\left(\frac{h_{FJ}}{Nl_k}\right)} \right] \tag{1}$$

$$L(x) = \coth x - \frac{1}{x} \tag{2}$$

where k_{FJ} is the constant, $h_{FJ} = \sqrt{\frac{I_1}{3}} (I_1 = \lambda_1^2 + \lambda_2^2 + \lambda_3^2)$ is the mean square end distance. λ_1, λ_2 and λ_3 represent the stretching ratios of the cubic hydrogels in three directions, respectively. *N* is the number of Kuhn segments, $L(x)$ is the contour length, and l_k is the length of Kuhn segment.

According to the equation (1), the stress (σ_{FJ}) obtained from the FJC model can be written as follows [41-43],

$$\sigma_{FJ} = N_{FJ} k_B T \frac{\lambda_i^2}{\left(1 - \frac{I_1}{3N}\right)\left(1 + \frac{I_1}{6N}\right)} + p_n \tag{3}$$

where N_{FJ} is the number of chains of stretchable network.

As there is a folding-to-unfolding transition in the stretchable network, the probabilities of folding (β_1) and unfolding (α_1) are presented as [35],

$$\beta_1 = \omega \exp\left(\frac{-\Delta G_f + f l_f}{k_B T}\right) \tag{4}$$

$$\alpha_1 = \omega \exp(\frac{-\Delta G_u + f l_u}{k_B T}) \tag{5}$$

where ΔG_f and ΔG_u are activation energies of folding and unfolding chains, respectively. l_f and l_u are the widths of the activation barrier in folding and unfolding states, respectively. ω is the normalized parameter, f is the force on a single chain, k_B is the Boltzmann constant and T is temperature. During the folding-to-unfolding transition, the total number of chains (N) in the stretchable network is kept a constant, e.g., $N = N_f + N_u$. According to equations (4) and (5), the number of folding chains (N_f) can be expressed as,

$$N_f = \frac{\beta_1}{\alpha_1 + \beta_1} N = \frac{1}{\exp(\frac{-\Delta G + f \Delta l}{k_B T}) + 1} N \tag{6}$$

where $\Delta G = \Delta G_u - \Delta G_f$ and $\Delta l = l_u - l_f$.

Based on the rubber elasticity theory [38-40], the stress of a single chain is determined by the mean square end distance (h), e.g.,

$$f = \frac{3 k_B T}{n l_b^2} h \quad \left(h = \sqrt{\frac{I_1}{3}} \text{ and } I_1 = \lambda_1^2 + \lambda_2^2 + \lambda_3^2 \right) \tag{7}$$

where n is the number of monomer and l_b is the monomer length.

Substituting equation (7) into (6), we can obtain:

$$N_f = \frac{1}{\exp(\frac{-\Delta G}{k_B T} + \frac{\sqrt{3}\Delta l}{n l_b^2} \sqrt{\lambda^2 + \frac{2}{\lambda}}) + 1} N \tag{8}$$

where $\lambda_1 = \lambda$ and $\lambda_2 = \lambda_3 = \lambda^{-1/2}$ in the uniaxial tensile test [38-40], according to assumption of volume invariance of isotropic materials, i.e., $\lambda_1 \lambda_2 \lambda_3 = 1$.

The total length of the chains (l_t) can be incorporated with the lengths of folding

and unfolding chains, thus it can be expressed as,

$$l_t = N_f l_f + N_u l_u = N l_u - \frac{\Delta l N}{\exp(\frac{-\Delta G}{k_B T} + \frac{\sqrt{3}\Delta l}{n l_b^2}\sqrt{\lambda^2 + \frac{2}{\lambda}}) + 1} \tag{9}$$

According to the scaling theory ($h \propto l$) [40] and rubber elasticity theory [38-40], the constitutive stress-strain relationship of the stretchable network can be written as,

$$\begin{aligned} \sigma_e &= N_e k_B T \frac{h_t^2}{h_0^2}(\lambda - \frac{1}{\lambda^2}) = N_e k_B T \frac{l_t^2}{l_0^2}(\lambda - \frac{1}{\lambda^2}) \\ &= \frac{N_e k_B T}{l_0^2}[N l_u - \frac{\Delta l N}{\exp(\frac{-\Delta G}{k_B T} + \frac{\sqrt{3}\Delta l}{n l_b^2}\sqrt{\lambda^2 + \frac{2}{\lambda}}) + 1}]^2(\lambda - \frac{1}{\lambda^2}) \end{aligned} \tag{10}$$

2.2 Mechanochemical transition of brittle network

For the brittle network in the DN hydrogel, there is a linear deformation behavior in response to external stress, thus the mechanical energy (H_{cm}) can be written using a format of Hooke's Law,

$$H_{cm} = \frac{1}{2} E_{cm}(\lambda - 1)^2 = G_h N_{cm} \tag{11}$$

where E_{cm} is the Young's modulus of hydrogel, G_h is the bond energy of brittle network and N_{cm} is the number of macromolecule chains undergoing mechanochemical transition in the brittle network. Under a uniaxial stretching, the stress of brittle network can be obtained in combination of equations (3) and (11),

$$\begin{aligned} \sigma_{FJ} &= (N_{FJ} - N_{cm}) k_B T \frac{\lambda_i^2}{(1 - \frac{I_1}{3N})(1 + \frac{I_1}{6N})} \\ &= [N_{FJ} - \frac{E_{cm}}{2G_h}(\lambda - 1)^2] k_B T \frac{\lambda^2 - \frac{1}{\lambda}}{(1 - \frac{\lambda^2 + \frac{2}{\lambda}}{3N})(1 + \frac{\lambda^2 + \frac{2}{\lambda}}{6N})} \end{aligned} \tag{12}$$

On the other hand, the mixing entropy has also been changed due to the

mechanochemical transition according to the Flory-Huggins solution theory [38-40]. During this transition, the mixture of brittle network and water has been changed into the mixture of broken macromolecule chains and water, thus resulting in the changes of mixing entropy. These changes in mixing entropy (ΔS_M) and mixing enthalpy ($\Delta H_M^{'}$) can be obtained using the following equations,

$$\Delta S_M = -Rn_1 \ln \phi_1 \tag{13}$$

$$\Delta H_M^{'} = \Delta H_M - \Delta H_{cm} = RT\chi n_1 \phi_2 - \frac{1}{2} E_{cm} (\lambda - 1)^2 \tag{14}$$

where R is the gas constant ($R = k_B N_A$, N_A is the Avogadro constant), ΔH_M is the mixing enthalpy, χ is the interaction parameter. Based on the equations (13) and (14), the mixing free energy (ΔW_M) can be further written as,

$$\Delta W_M = -(\Delta H_M^{'} - T\Delta S_M) = -RT\chi n_1 \phi_2 + \frac{1}{2} E_{cm} (\lambda - 1)^2 - RTn_1 \ln \phi_1 \tag{15}$$

where n_1 and ϕ_1 represent the molar and volume fractions of the hydrogel, respectively, ϕ_2 represent the volume fraction of water. It is assumed that the water molecules are incompressible, and increases of their volume fractions can increase volume of the hydrogel, thus, we can obtain $\phi_1 = \frac{1}{\lambda^3}$ and $\phi_2 = 1 - \frac{1}{\lambda^3}$.

Based on the equation (15), the stress can be expressed by,

$$\sigma_M = \frac{d\Delta W_M}{d\lambda} = 3RTn_1 (\frac{1}{\lambda} - \frac{\chi}{\lambda^4}) + E_{cm} (\lambda - 1) \tag{16}$$

2.3 Mechanical behavior of DN hydrogel

According to the equations (10), (12) and (16), the constitutive relationship of stress as a function of stretching ratio for the DN hydrogel can therefore be obtained,

$$\sigma = \sigma_e + \sigma_{FJ} + \sigma_M = [\frac{Nl_u\sqrt{N_e k_B T}}{l_0} - \frac{\Delta l N\sqrt{N_e k_B T}/l_0}{\exp(\frac{-\Delta G}{k_B T} + \frac{\sqrt{3}\Delta l}{n l_b^2}\sqrt{\lambda^2 + \frac{2}{\lambda}}) + 1}]^2(\lambda - \frac{1}{\lambda^2}) +$$
$$[N_{FJ} - \frac{E_{cm}}{2G_h}(\lambda - 1)^2]k_B T \frac{\lambda^2 - \frac{1}{\lambda}}{(1 - \frac{\lambda^2 + \frac{2}{\lambda}}{3N})(1 + \frac{\lambda^2 + \frac{2}{\lambda}}{6N})} + E_{cm}(\lambda - 1) + 3RTn_1(\frac{1}{\lambda} - \frac{\chi}{\lambda^4}) + p \quad (17)$$

where p is the hydrostatic pressure.

Using the above proposed model, the analytical results for the DN hydrogel have been plotted in Figure 2. All the parameters used in equation (17) are listed in Table 1. Here p=0 is hydrostatic pressure, and it is obtained from boundary condition when the initial stress is 0. As shown in Figure 2(a), the model can describe the overall mechanical process of the DN hydrogel, which undergoes three steps of deformation stages, e.g., linear elastic deformation, non-linear large deformation and mechanochemical transition. The stretchable network undergoes a non-linear and large deformation, which is governed by the folding-to-unfolding transition. Meanwhile, the pre-stretched brittle network undergoes a linear elastic deformation, followed by a mechanochemical transition, which are governed by the Hooke's Law and Flory-Huggins theory, respectively. Analytical results of the stress values as a function of elongation ratio are plotted in Figure 2(b), at a given length in change (Δl). The ultimate stress is gradually decreased from 1.05 MPa to 0.85 MPa, with an increase of the value of Δl from 1.5×10^{-3} to 3.9×10^{-3}. With a lower value of Δl, more mechanical energy is necessary to stretch the DN hydrogel at a constant elongation ratio. The length in change (Δl) of folding-to-unfolding transition plays a critical role to determine the mechanical behavior the DN hydrogel.

Table 1. Values of parameters used in equation (17), where the hydrostatic pressure p=0.

$\frac{l_u\sqrt{N_e k_B T}}{l_0}(MPa)^{0.5}$	$\frac{\sqrt{N_e k_B T}}{l_0}(MPa)^{0.5}$	$\frac{-\Delta G}{k_B T}$	$\frac{\sqrt{3}}{n l_b^2}$	$3RTn_1(MPa)$
1.58×10^{-3}	0.316	-1.0	33.33	0.5
$\frac{E_{cm}}{2G_h}k_B T(MPa)$	$N_{FJ}k_B T(MPa)$	$E_{cm}(MPa)$	χ	N
3×10^{-5}	4×10^{-3}	0.01	1.0	200

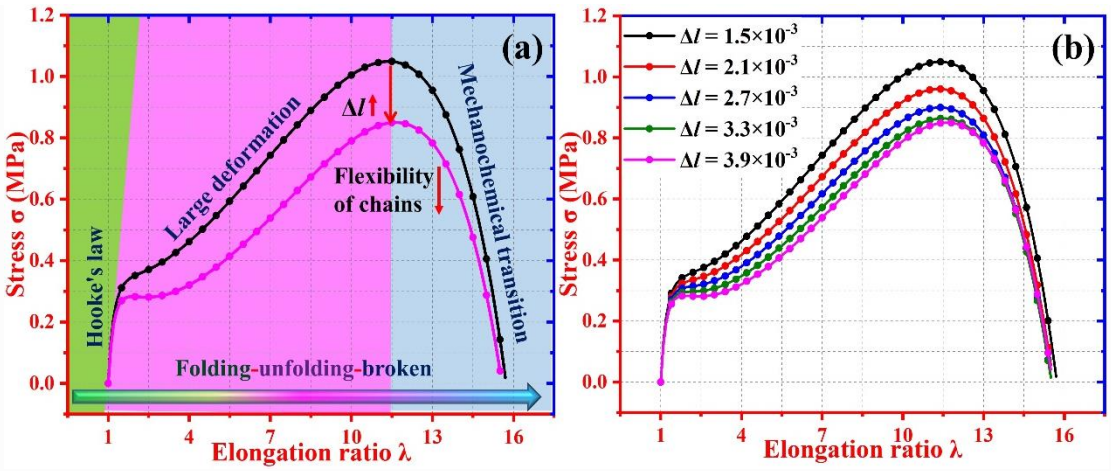

Figure 2. (a) Illustration of folding-to-unfolding and mechanochemical transitions. (b) Analytical results of stress *vs.* elongation ratio of DN hydrogel at given constants of Δl =1.5×10^{-3}, 2.1×10^{-3}, 2.7×10^{-3}, 3.3×10^{-3} and 3.9×10^{-3}.

2.4 Experimental verification

To verify the proposed model, two groups of experimental data reported in Refs. [25,48] for the DN hydrogels of PAMPS/PAAM (PAMPS: poly(2-Acrylamido-2-methylpropanesulfonic acid; PAAM: poly(Acrylamide)) and SF/SA-AMx (SF is silk fibroin, SA: stearyl acrylate, AM: acrylamide and x is the concentration of sodium dodecyl sulfate) have been employed to compare with the analytical results. Figure 3(a) plots the constitutive stress-elongation ratio relationship

of PAMPS/PAAM DN hydrogels with various concentrations of PAAM (C_W), e.g., 1.1M, 1.3M, 1.5M and 1.7 M (M: mole) [25], where the hydrostatic pressure *p*=0.076, 0.068, 0.052 and 0.056, respectively. All the parameters used in the calculation using the equation (17) are listed in Table 2, at given constants of $\frac{-\Delta G}{k_B T} = -1.2$, $\frac{\sqrt{3}}{n l_b^2} = 0.05$ and $\chi = 3$. It is found that the analytical results fit well with the experimental data. With the values of C_W increased from 1.1M, 1.3M, 1.5M to 1.7M, both the stress and mechanical energy are increased at the same elongation ratio. Furthermore, the obtained yield strengths are 0.21 MPa, 0.19 MPa, 0.14 MPa and 0.17 MPa. The similarities between the analytical and experimental results have been compared using the correlation index (R^2), and their values for the PAMPS/PAAM DN hydrogels with $C_W(M)$ of 1.1M, 1.3M, 1.5M and 1.7 M are 89.68%, 80.35%, 93.01% and 97.97%, respectively.

Experimental data of SF/SA-AMx DN hydrogels with a variety of concentrations of sodium dodecyl sulfate [48] have also been employed to compare with the analytical results based on the proposed model. From the results shown in Figure 3(b), the theoretical model can well predict the constitutive relationship of stress with respect to elongation ratio for the SF/SA-AMx DN hydrogels. All the parameters used in calculations based on the equation (17) are listed in Table 2, at given constants of $\frac{-\Delta G}{k_B T} = -1.2$, $\frac{\sqrt{3}}{n l_b^2} = 0.05$ and $\chi = 1$. Furthermore, the yield strengths were also calculated and they are 0.093 MPa, 0.141 MPa and 0.112 MPa for the DN hydrogels with concentrations of sodium dodecyl sulfate of 1/8, 1/16 and 1/20, respectively. The

similarities between the analytical and experimental results have been obtained, and the correlation index (R^2) are 98.47%, 98.85% and 98.66%, for the SF/SA-AMx DN hydrogels with concentrations of sodium dodecyl sulfate of 1/8, 1/16 and 1/20, respectively.

Table 2. Values of parameters used in equation (17) for PAMPS/PAAM and SF/SA-AMx DN hydrogels.

	$\frac{\sqrt{N_e k_B T}}{l_0 / l_u}$	$\frac{\sqrt{N_e k_B T}}{l_0 / \Delta l}$	$N_{FJ} k_B T$	$\frac{E_{cm}}{2G_h} k_B T$	E_{cm}	N	$3RTn_1$
1.1M	1.85×10^{-4}	5.55×10^{-5}	5.0×10^{-5}	5.0×10^{-8}	2.0×10^{-3}	310	0.38
1.3M	3.01×10^{-4}	9.09×10^{-5}	9.0×10^{-5}	9.0×10^{-8}	2.3×10^{-3}	210	0.36
1.5M	2.75×10^{-4}	8.23×10^{-5}	6.5×10^{-5}	6.5×10^{-8}	2.0×10^{-3}	215	0.26
1.7M	4.26×10^{-4}	1.28×10^{-4}	1.6×10^{-4}	1.6×10^{-7}	2.0×10^{-3}	210	0.31
AM1/8	3.69×10^{-3}	2.21×10^{-3}	3.0×10^{-3}	3.8×10^{-5}	5.0×10^{-3}		0.12
AM1/16	4.01×10^{-3}	2.01×10^{-3}	3.2×10^{-3}	2.7×10^{-5}	1.0×10^{-2}	160	0.20
AM1/20	3.54×10^{-3}	1.77×10^{-3}	2.4×10^{-3}	2.0×10^{-5}	1.0×10^{-2}		0.16

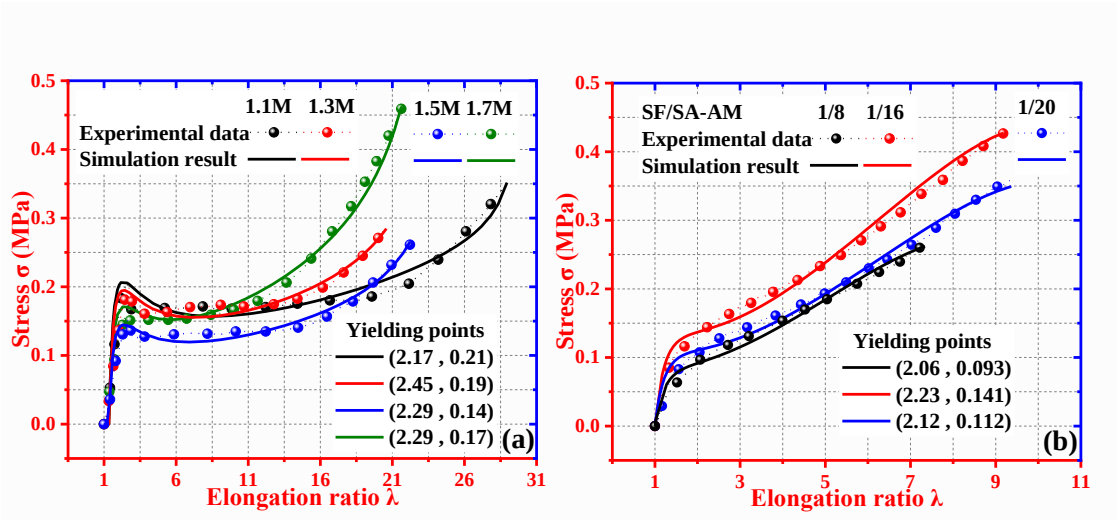

Figure 3. (a) Comparisons of analytical results and experimental data [25] for the PAMPS/PAAM DN hydrogels with various concentrations of PAAM. (b) Comparisons of analytical results and experimental data [48] for the SF/SA-AMx DN hydrogels with various concentrations of sodium dodecyl sulfate.

3. Modelling of polyampholyte DN hydrogel

3.1 Modeling of entanglement and dangling effects

For the DN hydrogel, the stretchable network undergoes a folding-to-unfolding transition in response to an external force [35-37]. While the brittle network undergoes a mechanochemical transition to resist the external force. If these two networks have the opposite electrical charges, they could form either strong or weak bonds among the macromolecule chains [27-30], in which the strong bonds are due to the crosslinks by means of chain-poly[n]-entanglements [27,28], whereas the weak bonds are due to the broken dangling chains with the opposite charges, as shown in Figure 4(a). In comparison with the conventional DN hydrogels, polyampholyte ones present a unique enhancement effect due to the charge attraction between these two different networks [27-30]. However, there are two types of charge attractions based on the bonding strengths, i.e. a strong bonding associated to the entanglement effect and a weak bonding associated to the dangling effect, as shown in Figure 4(b).

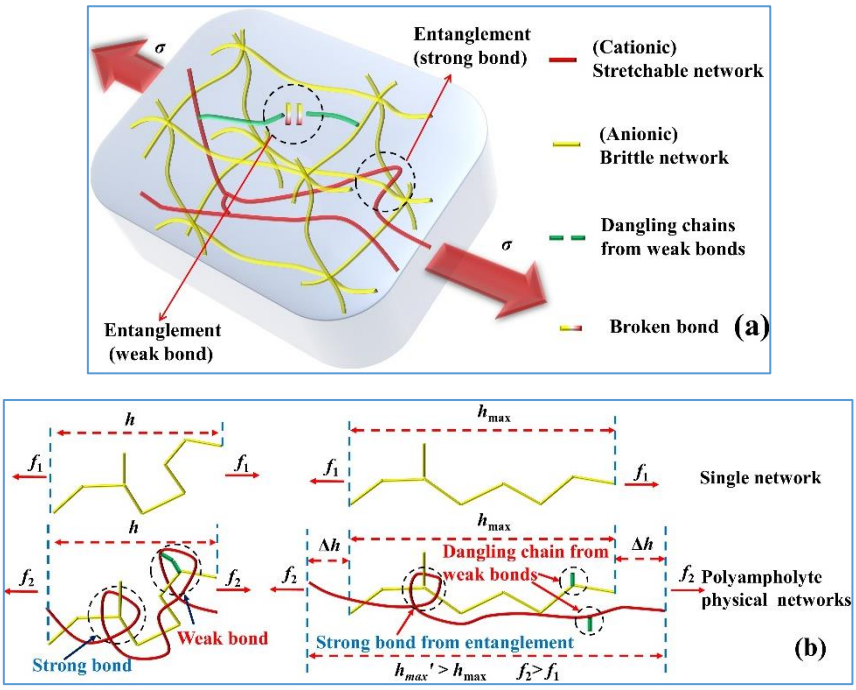

Figure 4. (a) Schematic illustration of mechanoresponsive behaviors of networks in the polyampholyte DN hydrogel. (b) Schematic illustration of the stress-induced entanglement and dangling effects in polyampholyte DN hydrogel.

Here the WLC model is applied to characterize the free energy (F_{wl}) and stress (σ_{wl}) functions of entanglement effect in the polyampholyte DN hydrogel [37],

$$F_{wl} = -N_{wl}k_BT\ln\Omega_{wl} = N_{wl}k_BT\{\ln\frac{k_{wl}}{L_{wl}} - \frac{9}{2}\ln[1-(\frac{h_{wl}}{L_{wl}})^2] - \frac{-3L_{wl}}{4l_p(1-\frac{h_{wl}}{L_{wl}})^2}\} \quad (18a)$$

$$\sigma_{wl} = \frac{\partial F_{wl}}{\partial\lambda} = N_{wl}k_BT[\frac{9\frac{h_{wl}}{L_{wl}^2}}{1-(\frac{h_{wl}}{L_{wl}})^2} + \frac{3}{2l_p(1-\frac{h_{wl}}{L_{wl}})^3}]\frac{\partial h_{wl}}{\partial\lambda} \quad (18b)$$

where N_{wl} is the number of chains involved into entanglement effect, k_{wl} is a constant, h_{wl} is the mean square end distance, L_{wl} is the contour length and l_p is the persistence length.

Furthermore, the dangling effect can be described using the tube model [40], thus, tube mobility (μ_{tu}) and diffusion coefficient (D_{tu}) can be written as,

$$\mu_{tu} = \frac{v_{tu}}{f_{tu}} = \frac{\mu_1}{N_{tu}} \tag{19a}$$

$$D_{tu} = \mu_{tu} k_B T = \frac{\mu_1 k_B T}{N_{tu}} \tag{19b}$$

where v_{tu} is the relaxation velocity of chain, f_{tu} is the equivalent friction, N_{tu} is the number of chains and μ_1 is a constant. According to the tube model [40], the relaxation time (τ_{tu}) can be expressed as,

$$\tau_{tu} \approx \frac{L_{wl}^2}{D_{tu}} = \frac{N_{tu} L_{wl}^2}{\mu_1 k_B T} \propto N_{tu}^3 = \frac{k_{tu}}{T} N_{tu}^3 \tag{20}$$

where k_{tu} is the scaling parameter [40].

Based on the equations (19) and (20), two different networks are considered to become mutual if there is neither externally mechanical loading nor charge attraction during their entanglements, thus, it has an relaxation velocity of $v_{tu} = \frac{L_{wl}}{\tau_{tu}} = \frac{\mu_1 k_B T}{N_{tu} L_{wl}}$. Here the force (f_{wl}) caused by entanglement effect can be expressed by,

$$f_{wl} = f_{tu} = \frac{v_{tu} N_{tu}}{\mu_1} = \frac{k_B T}{L_{wl}} \tag{21}$$

A correction of stress-strain relationship caused by the strong entanglement is introduced as [35,36],

$$\begin{cases} f_{wl} \dfrac{l_p}{k_B T} = \dfrac{l_p}{L_{wl}} = \dfrac{1}{4(1-\dfrac{\Delta h}{L_{wl}})^2} + \dfrac{\Delta h}{L_{wl}} - \dfrac{1}{4} & \left(\Delta h = \dfrac{2 l_p}{3}\right) \\ \dfrac{1}{4(1-\dfrac{\Delta h}{L_{wl}})^2} \approx \dfrac{1}{4} + \dfrac{1}{2}\dfrac{\Delta h}{L_{wl}} + o(\dfrac{\Delta h}{L_{wl}})^2 & \left(\dfrac{\Delta h}{L_{wl}} \ll 1\right) \end{cases} \tag{22}$$

where Δh is the mean square end distance of strong bond.

The mean square end distances of entanglement ($\left(h_{wl}+\Delta h\right)/h_{wl}$) and macromolecule chain ($h_{wl}^2 = 2l_p(L_{wl}-l_p)$ [36,38,39]) can be further expressed, respectively, as,

$$\frac{h_{wl}+\Delta h}{h_{wl}} = \frac{\sqrt{\frac{L_{wl}}{l_p}-1}+\frac{\sqrt{2}}{3}}{\sqrt{\frac{L_{wl}}{l_p}-1}} = 1+\frac{1}{3}\sqrt{\frac{2l_p}{|L_{wl}-l_p|}} \tag{23a}$$

$$h_{wl} = \frac{1}{1+\frac{1}{3}\sqrt{\frac{2l_p}{|L_{wl}-l_p|}}}\sqrt{\frac{I_1}{3}} \quad \left(I_1=\lambda_1^2+\lambda_2^2+\lambda_3^2\right) \tag{23b}$$

On the other hand, effect of weak bonding on mechanical behavior is governed by the dangling chain theory [40]. The relaxation behavior of dangling chain is governed by the rubber elasticity theory and can be written as [38-40],

$$N_d \cong k_{d1}\ln(\frac{t}{\tau_d}) \tag{24a}$$

$$\sigma_d = -k_B T[k_{d1}\ln(\frac{\lambda-1}{\tau_d})-k_{d2}\ln(\dot{\lambda})](\lambda-\frac{1}{\lambda^2}) \tag{24b}$$

where N_d is the number of dangling chains, τ_d is relaxation time of a dangling chain, k_{d1} and k_{d2} are normalized parameters associated to the numbers of dangling chains [40].

According to equations (18), (20) and (24), the constitutive stress-elongation ratio relationship can be written using the extended Maxwell model [34],

$$\sigma_{tu} = \dot{\lambda}k_B N_{tu} T\tau_{tu}[1-\exp(-\frac{\lambda-1}{\dot{\lambda}\tau_{tu}})] \tag{25a}$$

$$\sigma=\sigma_{wl}+\sigma_{tu}+\sigma_{d}=N_{wl}k_{B}T[\frac{9\frac{h_{wl}}{L_{wl}^{2}}}{1-(\frac{h_{wl}}{L_{wl}})^{2}}+\frac{3}{2l_{p}(1-\frac{h_{wl}}{L_{wl}})^{3}}]\frac{\partial h_{wl}}{\partial\lambda}$$
$$+\dot{\lambda}k_{B}N_{tu}^{4}k_{tu}[1-\exp(-\frac{(\lambda-1)T}{\dot{\lambda}N_{tu}^{3}k_{tu}})]-k_{B}T[k_{d1}\ln(\frac{\lambda-1}{\tau_{d}})-k_{d2}\ln(\dot{\lambda})](\lambda-\frac{1}{\lambda^{2}}) \quad (25b)$$

where $\dot{\lambda}$ is the loading rate. Under the uniaxial tension loading ($\lambda_1=\lambda$ $\lambda_2=\lambda_3=\lambda^{-1/2}$ $I_1=\lambda^2+2\lambda^{-1}$) and shearing loading ($\lambda_1=\lambda$ $\lambda_2=1$ $\lambda_3=\lambda^{-1}$ $I_1=\lambda^2+\lambda^{-2}+1$), the constitutive relationship of stresses can be written as follows,

$$\sigma_1=(\sigma_{wl}+\sigma_{tu}+\sigma_{d})|_{I_1=\lambda^2+2\lambda^{-1}}=$$
$$[\frac{\frac{9\sqrt{\lambda^2+\frac{2}{\lambda}}}{3+\sqrt{\frac{2l_p}{|L_{wl}-l_p|}}}\frac{1}{L_{wl}^{2}}}{1-(\frac{\sqrt{3}\sqrt{\lambda^2+\frac{2}{\lambda}}}{3+\sqrt{\frac{2l_p}{|L_{wl}-l_p|}}}\frac{1}{L_{wl}})^{2}}+\frac{1/2l_p}{(1-\frac{\sqrt{3}\sqrt{\lambda^2+\frac{2}{\lambda}}}{3+\sqrt{\frac{2l_p}{|L_{wl}-l_p|}}}\frac{1}{L_{wl}})^{3}}]\frac{3\sqrt{3}N_{wl}k_{B}T(\lambda-\frac{1}{\lambda^{2}})}{(3+\sqrt{\frac{2l_p}{|L_{wl}-l_p|}})\sqrt{\lambda^2+\frac{2}{\lambda}}} \quad (26a)$$
$$+\dot{\lambda}k_{B}N_{tu}^{4}k_{tu}[1-\exp(-\frac{(\lambda-1)T}{\dot{\lambda}N_{tu}^{3}k_{tu}})]-k_{B}T[k_{d1}\ln(\frac{\lambda-1}{\tau_{d}})-k_{d2}\ln(\dot{\lambda})](\lambda-\frac{1}{\lambda^{2}})$$

$$\sigma_{sh}=(\sigma_{wl}+\sigma_{tu}+\sigma_{d})|_{I_1=\lambda^2+\lambda^{-2}+1}=$$
$$[\frac{\frac{9\sqrt{I_1}}{3+\sqrt{\frac{2l_p}{|L_{wl}-l_p|}}}\frac{1}{L_{wl}^{2}}}{1-(\frac{\sqrt{3}\sqrt{I_1}}{3+\sqrt{\frac{2l_p}{|L_{wl}-l_p|}}}\frac{1}{L_{wl}})^{2}}+\frac{1/2l_p}{(1-\frac{\sqrt{3}\sqrt{I_1}}{3+\sqrt{\frac{2l_p}{|L_{wl}-l_p|}}}\frac{1}{L_{wl}})^{3}}]\frac{\sqrt{3}N_{wl}k_{B}T(\lambda-\frac{1}{\lambda^{3}})}{(3+\sqrt{\frac{2l_p}{|L_{wl}-l_p|}})\sqrt{I_1}} \quad (26b)$$
$$+\dot{\lambda}k_{B}N_{tu}^{4}k_{tu}[1-\exp(-\frac{(\lambda-1)T}{\dot{\lambda}N_{tu}^{3}k_{tu}})]-k_{B}T[k_{d1}\ln(\frac{\lambda-1}{\tau_{d}})-k_{d2}\ln(\dot{\lambda})](\lambda-\frac{1}{\lambda^{2}})$$

For the unloading process, the weak bonds take a certain relaxation time to regain their original state, thus, the constitutive stress relationship shows a time-dependent behavior,

$$\sigma_{unloading} = \sigma_{tu} = \dot{\lambda} k_B N_{tu}^4 k_{tu} [1 - \exp(-\frac{(\lambda - \lambda_r)T}{\dot{\lambda} N_{tu}^3 k_{tu}})] \quad (27)$$

where $\dot{\lambda}$ is the stretching rate and λ_r is the residual elongation ratio in the cyclically process.

To verify the model of entanglement and dangling effects in polyampholyte DN hydrogels, the constitutive stress-elongation ratio relationship was further investigated to explore their working mechanisms of mechanical behaviors. Based on the proposed model of equation (26), the analytical results of polyampholyte DN hydrogel were obtained, and the results are plotted in Figure 5. All the parameters used in the calculation using the equation (26) are listed in Table 3. In comparison with those of the conventional DN hydrogels, both yield strength and elongation ratio of the polyampholyte DN hydrogels have been significantly increased due to the entanglement and dangling effects, as shown in Figure 5(a). Due to the charge attraction, a high mechanical energy is needed for the polyampholyte DN hydrogel to resist the entanglement and dangling effects, which are originated from the strong and weak bonds of polyampholyte networks, respectively.

Table 3. Values of parameters used in equation (26).

l_p	L_{wl}	$N_{wl}k_BT(MPa)$	$k_BN_{tu}^4k_{tu}(MPa\cdot s)$	$\frac{T}{N_{tu}^3k_{tu}}(s^{-1})$
1	12	0.8	4	0.02
$\tau_d(s)$	$k_{d1}k_BT(MPa)$	$k_{d2}k_BT(MPa)$	$\dot{\lambda}(s^{-1})$	
7.39	0.1	0.1	1	

Furthermore, the analytical results also indicate that the entanglement effect plays a more significant role to enhance the mechanical strength of the polyampholyte DN

hydrogel, in comparison with that of the dangling effect. Figure 5(b) is plotted to illustrate the entanglement effect as a function of flexibility ($\frac{l_p}{L_{wl}}$) of macromolecule chain. The entanglement effect reaches its maximum value with an increase in flexibility from $\frac{l_p}{L_{wl}}$=0 to $\frac{l_p}{L_{wl}}$=1. However, it is then gradually decreased with a further increase in flexibility.

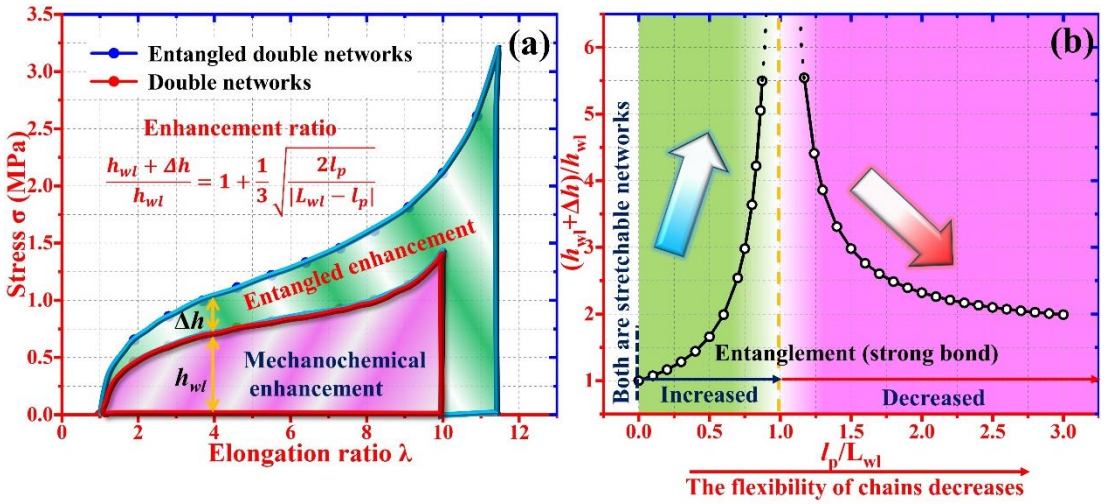

Figure 5. Analytical results of equations (23) and (26). (a) Stress-elongation ratio behavior of polyampholyte and conventional DN hydrogels. (b) The mean square end distance of entanglement effect ($\frac{h_{wl}+\Delta h}{h_{wl}}$) with respect to flexibility ($\frac{l_p}{L_{wl}}$) of macromolecule chain.

Analytical results of the stress values as a function of elongation ratio at different relaxation times (τ_d) of 3.669 s, 4.482 s, 5.474 s, 6.686 s and 8.166 s are plotted in Figure 6. These analytical results can be explained by the tube model [40]. Figure 6(a) shows the effect of diameter of tube on the stress and dangling relaxation of DN hydrogel. With a larger diameter of the tube, the dangling chains are more difficult to

relax, thus resulting in a higher mechanical energy and stress to resist the externally mechanical loading. That is to say, all the functions that determine the diameter of tube will therefore influence the dangling relaxation and mechanical behavior of the polyampholyte DN hydrogels.

On the other hand, the analytical results of the stress as a function of relaxation time (τ_d) are plotted in Figure 6(b). With an increase in the relaxation time (τ_d) from 3.669 s to 8.166 s, the stress is dramatically increased from 1.42 MPa to 2.22 MPa at the same elongation ratio of λ=10. These analytical results can also be explained by the tube model [40]. With an increase in relaxation time, the diameter of the tube is therefore increased, thus causing the increased recovery ratio of dangling chains. Therefore, the relaxation motion of dangling chains is then significantly restricted, thus resulting in the enhanced mechanical energy and stress.

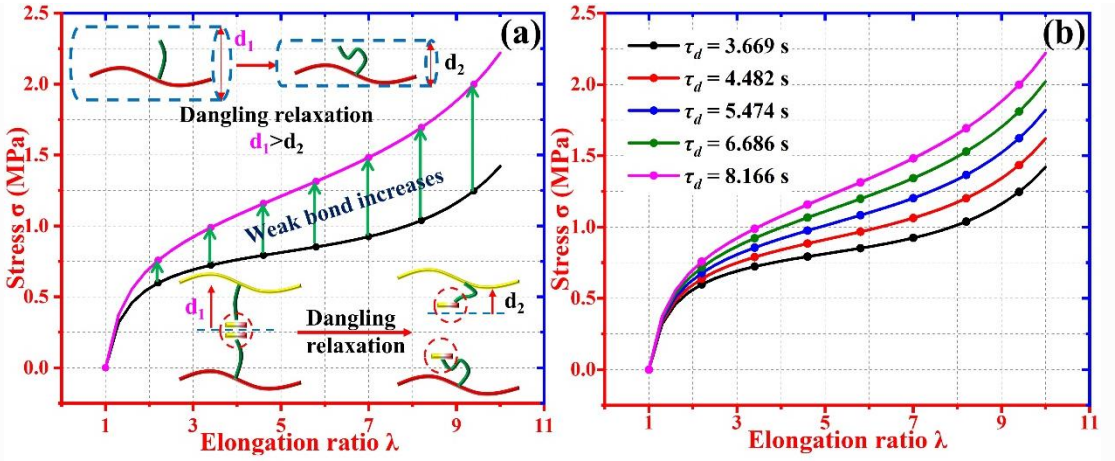

Figure 6. Analytical results of equation (26) for dangling effect in polyampholyte DN hydrogel. (a) Effect of diameter of tube on constitutive stress-elongation ratio relationship. (b) Effect of relaxation time (τ_d) on constitutive stress-elongation ratio relationship at τ_d=3.669 s, 4.482 s, 5.474 s, 6.686 s and 8.166 s.

3.2 Experimental verification

To verify the proposed model based on equation (26a), the analytical results of effect of stretching rate on constitutive stress-elongation ratio relationship have been plotted in Figure 7, together with the experimental data of polyampholyte poly(NaSS-co-MPTC) (NaSS: sodium *p*-styrenesulfonate; MPTC: 3-(methacryloylamino) propyltrimethylammonium chloride) DN hydrogel, reported in Ref. [29]. The parameters used in the equation (26a) are listed in Table 4.

Table 4. Values of parameters used in equation (26a) for polyampholyte poly(NaSS-co-MPTC) DN hydrogel at a variety of stretch rate.

$\dot{\lambda}(s^{-1})$	L_{wl}	l_p	$N_{wl}k_BT$	$k_BN_{tu}^4k_{tu}$	$\frac{T}{N_{tu}^3k_{tu}}$	$k_{d1}k_BT$	$k_{d2}k_BT$	τ_d
0.01	8.6	1.25	7.532	330	8.0×10^{-3}	1.321	0.736	8.339
0.02	8.0		6.641	291		1.785		
0.1	9.0		7.873	345		2.484		
0.2	9.0		7.873	345		2.484		
0.41	9.0		9.413	402		2.969		

It is clearly seen from Figure 7 that the analytical results are in good agreements with the experimental ones. The similarities between the analytical and experimental results are compared using correlation index (R^2), which are 96.25%, 97.78%, 96.09%, 99.41% and 97.02% at the different stretching rates ($\dot{\lambda}$) of 0.01 s^{-1}, 0.02 s^{-1}, 0.1 s^{-1}, 0.2 s^{-1} and 0.41 s^{-1}, respectively. These analytical and experimental results reveal that the externally mechanical force is gradually increased with an increase in

the stretching rate ($\dot{\lambda}$) from 0.01 s^{-1}, 0.02 s^{-1}, 0.1 s^{-1}, 0.2 s^{-1} to 0.41 s^{-1}, at the same elongation ratio. The stretching rate plays a critical role to determine the rate-dependent mechanical behavior, which is resulted from the relaxation of dangling chains in the polyampholyte poly(NaSS-co-MPTC) DN hydrogel. Meanwhile, Figure 7(b) shows the simulation result using one set of parameters listed in Table 4, where $\dot{\lambda} = 0.01 s^{-1}$.

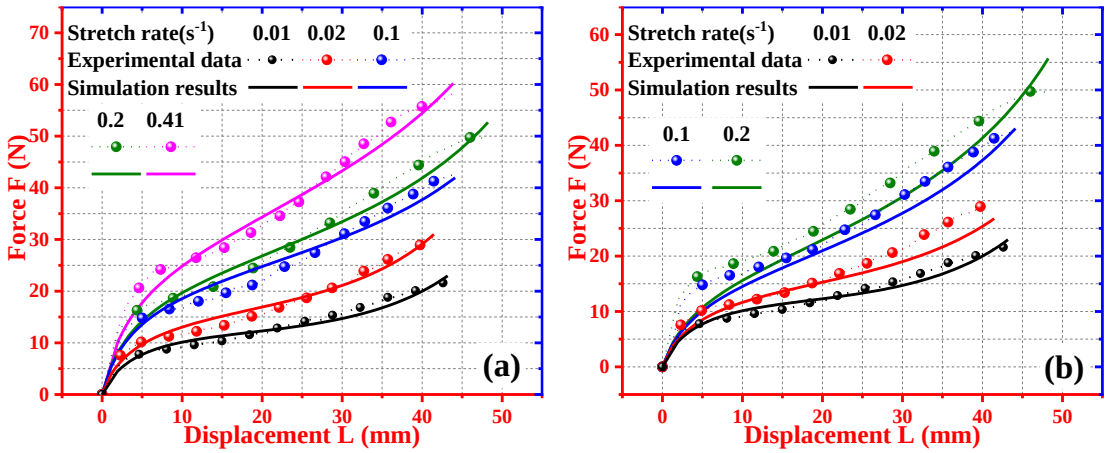

Figure 7. Comparisons of analytical and experimental results [29] for the force as a function of displacement of polyampholyte poly(NaSS-co-MPTC) DN hydrogel. (a) Based on different parameters as shown in Table 4. (b) Based on one set of parameters in Table 4, where $\dot{\lambda} = 0.01 s^{-1}$.

Meanwhile, effect of tearing rate on the mechanical behavior of the polyampholyte PNaSS-co-PMPTC DN hydrogel [30] was also investigated. The parameters used in the equation (26b) are listed in Table 5. Figure 8 plots the obtained constitutive stress-elongation ratio relationship of polyampholyte PNaSS-co-PMPTC DN hydrogel at various tearing rates. These analytical results fit well with the experimental data at the tearing rates ($\dot{\lambda}$) of 1.7×10^{-4} m/s, 1.7×10^{-3} m/s and 8.5×10^{-3} m/s [30]. With tearing rates increased from 1.7×10^{-4} m/s to 8.5×10^{-3} m/s, the tearing

force is significantly increased. Meanwhile, the similarities between the analytical and experimental results were calculated based on correlation index (R^2), which are 82.91%, 92.49% and 79.35% at the tearing rates ($\dot{\lambda}$) of 1.7×10^{-4} m/s, 1.7×10^{-3} m/s and 8.5×10^{-3} m/s, respectively.

Table 5. Values of parameters used in equation (26b) for polyampholyte PNaSS-co-PMPTC DN hydrogel at various tearing rates.

$\dot{\lambda}(m/s)$	L_{wl}	l_p	$N_{wl}k_BT$	$k_BN_{tu}^4k_{tu}$	$\frac{T}{N_{tu}^3k_{tu}}$	$k_{d1}k_BT$	$k_{d2}k_BT$	τ_d
0.17×10^{-3}	25	2.5	0.505	1788.23	2.353	1.6×10^{-3}	6×10^{-4}	4.056
1.7×10^{-3}	20		0.331	1095.29		6.9×10^{-2}		
8.5×10^{-3}	20		0.445	1475.29		1.7×10^{-1}		

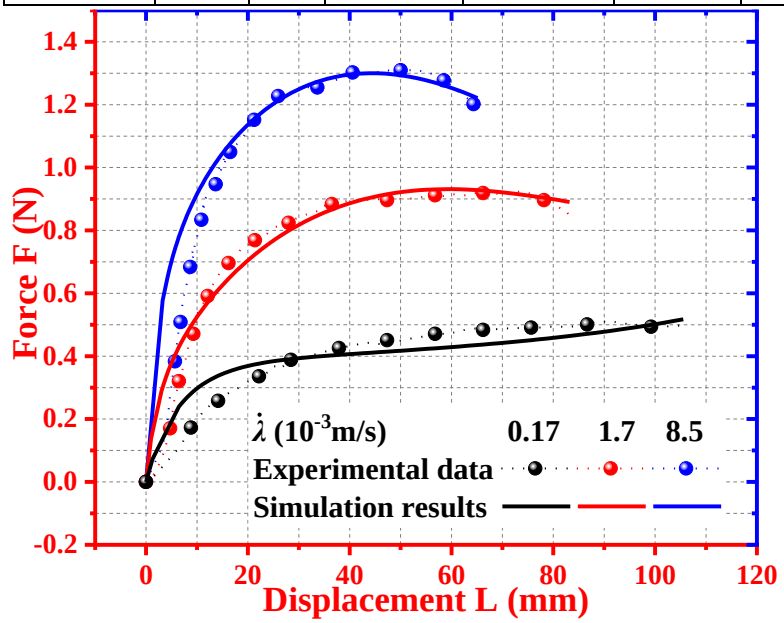

Figure 8. Comparisons of analytical results and experimental data [30] for the force as a function of displacement of polyampholyte DN hydrogels at a given tearing rate ($\dot{\lambda}$) of 1.7×10^{-4} m/s, 1.7×10^{-3} m/s and 8.5×10^{-3} m/s.

Finally, three groups of cyclic tensile experimental data [30] of polyampholyte

PNaSS-co-PMPTC DN hydrogel at different tensile strain rates have been employed to verify the analytical results using equations (26) and (27), which are plotted in Figure 9. All the parameters used in the equations (26) and (27) are listed in Table 6.

Table 6. Values of parameters used in equations (26) and (27) for polyampholyte PNaSS-co-PMPTC DN hydrogel in the cyclically mechanical loading, at given constants of l_p=1 and τ_d=1.235.

$\dot{\lambda}(s^{-1})$	L_{wl}	$N_{wl}k_BT$	$k_BN_{tu}^4k_{tu}$	$\frac{T}{N_{tu}^3k_{tu}}$	$k_{d1}k_BT$	$k_{d2}k_BT$	λ_r
0.014	5	0.0942	**1.857**/**6.428**	**0.14**/**0.04**	0.0309	1.03×10^{-2}	2.01
0.14	4	0.0843	**1.783**/**0.736**	**0.14**/**0.29**	0.1440	9.6×10^{-3}	2.20
0.69	4	0.1071	**2.652**/**0.088**	**0.14**/**0.89**	0.2806	9.6×10^{-3}	2.25

The stress is gradually increased with an increase in the elongation ratio. Both the analytical and experimental results show that the stress of polyampholyte PNaSS-co-PMPTC DN hydrogel is significantly increased from 0.178 MPa, 0.452 MPa to 0.816 MPa, with an increase in the strain rate ($\dot{\lambda}$) from 0.014 s^{-1}, 0.14 s^{-1} to 0.69 s^{-1}. With a high strain rate, the relaxation time of dangling chain is reduced and the diameter of tube becomes enlarged, thus resulting in increased mechanical energies and stresses due to the relaxation of dangling chains. Meanwhile, the residual elongation ratio (λ_r) is also increased from 2.01, 2.20 to 2.25 with an increase in the strain rate, thus resulting in increased relaxation time of dangling chains. Furthermore, according to the reversible mechanical behaviors of polyampholyte PNaSS-co-PMPTC DN hydrogel [30], the folding-to-unfolding transition of stretchable network, mechanochemical transition of brittle network, the entanglement

and dangling effects of polyampholyte macromolecule chains all have good reversibly mechanoresponsive properties.

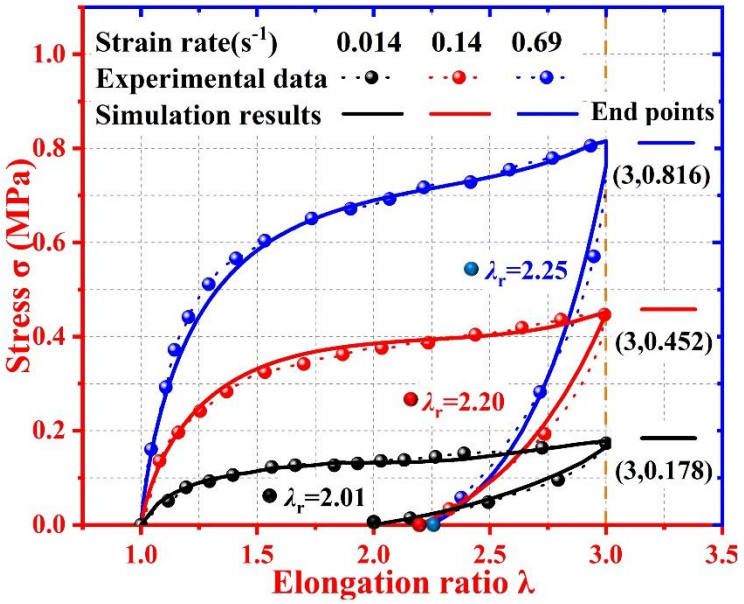

Figure 9. Comparisons of analytical results and experimental data [30] for the stress as a function of elongation ratio of polyampholyte PNaSS-co-PMPTC DN hydrogel at strain rates ($\dot{\lambda}$) of 014 s^{-1}, 0.14 s^{-1} and 0.69 s^{-1}.

4. Conclusions

In this study, we propose a collective and cooperative constitutive model to study the mechanical behavior of the polyampholyte DN hydrogels, which undergo folding-to-unfolding, mechanomechanical transitions, entanglement and dangling chain-poly[n]-catenations. The theoretical models have been developed to investigate and explain the working mechanisms of significantly improved mechanical behavior of polyampholyte DN hydrogels. It is demonstrated that the proposed framework is able to well predict constitutive stress-elongation ratio relationship, as functions of flexibility of macromolecule chain, diameter of dangling chain, stretching rate and tearing rate. Entanglement and dangling chain-poly[n]-catenations have been found to play an essential role to improve the mechanical properties of polyampholyte DN

hydrogels in comparison with these conventional ones. Finally, the analytical results have been verified using the experimentally obtained results reported in literature. This study is expected to provide a fundamental approach to formulate the constitutive relationship in polyampholyte DN hydrogel with an extremely high mechanical strength.

Acknowledgements

This work was financially supported by the National Natural Science Foundation of China (NSFC) under Grant No. 11725208, Newton Mobility Grant (IE161019) through Royal Society and NFSC.

References

[1] Lin P, Ma S H, Wang X L and Zhou F 2015 Molecularly engineered dual-crosslinked hydrogel with ultrahigh mechanical strength, toughness and good self-recovery *Adv. Mater.* **27** 2054-9

[2] Hu Y, Du Z S, Deng X L, Wang T, Yang Z H, Zhou W Y and Wang C Y 2016 Dual physically cross-linked hydrogels with high stretchability, toughness, and good self-recoverability *Macromolecules* **49** 5660-8

[3] Dai X Y, Zhang Y Y, Gao L N, Bai T, Wang W, Cui Y L and Liu W G 2015 A mechanically strong, highly stable, thermoplastic, and self-healable supramolecular polymer hydrogel *Adv. Mater.* **27** 3566-71

[4] Yuk H W, Zhang T, Lin S T, Parada G A and Zhao X H 2016 Tough bonding of hydrogels to diverse non-porous surfaces *Nat. Mater.* **15** 190-6

[5] Yang C, Liu Z, Chen C, Shi K, Zhang L, Ju X J, Wang W, Xie R and Chu L Y 2017 Reduced graphene oxide-containing smart hydrogels with excellent electro-response and mechanical properties for soft actuators *ACS Appl. Mater. Inter.* **9** 15758-67

[6] Fuhrer R, Athanassiou E K, Luechinger N A and Stark W J 2009 Crosslinking metal nanoparticles into the polymer backbone of hydrogels enables preparation of soft, magnetic field-driven actuators with muscle-like flexibility *Small* **5** 383-8

[7] Zheng W J, An N, Yang J H, Zhou J X and Chen Y M 2015 Tough Al-alginate/Poly(N-isopropylacrylamide) hydrogel with tunable LCST for soft robotics *ACS Appl. Mater. Interfaces* **7** 1758-64

[8] Webber R E, Creton C, Brown H R and Gong J P 2007 Large strain hysteresis and mullins effect of tough double-network hydrogels *Macromolecules* **40** 2919-27

[9] Jang S S, Goddard W A and Kalani M Y S 2007 Mechanical and transport properties of the poly (ethylene oxide)-poly (acrylic acid) double network hydrogel from molecular dynamic simulations *J. Phys. Chem. B* **111** 1729-37

[10] Kwon H J, Yasuda K, Ohmiya Y, Honma K, Chen Y M and Gong J P 2010 In vitro differentiation of chondrogenic ATDC5 cells is enhanced by culturing on synthetic hydrogels with various charge densities *Acta Biomater.* **6** 494-501

[11] Gong J P, Katsuyama Y, Kurokawa T and Osada Y 2003 Double-network hydrogels with extremely high mechanical strength *Adv. Mater.* **15** 1155-8

[12] Matsuda T, Nakajima T and Gong J P 2019 Fabrication of tough and stretchable hybrid double-network elastomers using ionic dissociation of polyelectrolyte in nonaqueous media *Chem. Mater.* **31** 3766-76

[13] Gong J P 2010 Why are double network hydrogels so tough? *Soft Matter* **6** 2583-90

[14] Yue Y F, Li X F, Kurokawa T and Gong J P 2016 Decoupling dual-stimuli responses in patterned lamellar hydrogels as photonic sensors *J. Mater. Chem. B.* **4** 4104-09

[15] Szheng S J, Li Z Q and Liu Z S 2019 The inhomogeneous diffusion of chemically crosslinked Polyacrylamide hydrogel based on poroviscosity theory *Sci. China Technol. SC.* **62** 1375-1384

[16] Zhao Y J, Zhao K Y, Li Y, Liu L, Zhang X X, Li J G, Chen M and Wang X L 2018 Enrichment of Cd^{2+} from water with a calcium alginate hydrogel filtration membrane *Sci. China Technol. SC.* **61** 438-445

[17] Lu H B, Shi X J, Yu K and Fu Y Q 2019 A strategy for modelling mechanochemically induced unzipping and scission of chemical bonds in double-network polymer composite *Compos. Part B* **165** 456-66

[18] Koetting M C and Peters J T 2015 Stimulus-responsive hydrogels: Theory, modern advances, and applications *Mat. Sci. Eng. R* **93** 1-49

[19] Hong W, Zhao X H and Suo Z G 2010 Large deformation and electrochemistry of polyelectrolyte gels *J. Mech. Phys. Solids* **58** 558-77

[20] Marcombe R and Cai S Q 2010 A theory of constrained swelling of a pH-sensitive hydrogel *Soft Matter* **6** 784-93

[21] Li J Y, Suo Z G and Vlassak J J 2014 A model of ideal elastomeric gels for polyelectrolyte gels *Soft Matter* **10** 2582-90

[22] Basak D and Ghosh S 2013 PH-regulated controlled swelling and sustained release from the core functionalized amphiphilic block copolymer micelle *ACS Macro Lett.* **2** 799-804

[23] Nakajima T, Takedomi N and Kurokawa T 2010 A facile method for synthesizing free-shaped and tough double network hydrogels using physically crosslinked poly(vinyl alcohol) as an internal mold *Polym. Chem.* **1** 693-7

[24] Tao L C, Sun L and Cui K P 2019 Facile synthesis of novel elastomers with tunable dynamics for toughness, self-healing and adhesion *J. Mater. Chem. A* **7** 17334-49

[25] Ahmed S, Nakajima T, Kurokawa K, Haque M A and Gong J P 2014 Brittleeductile transition of double network hydrogels: Mechanical balance of two networks as the key factor *Polymer* **55** 914-23

[26] Ilyas M, Haque M A and Yue Y F 2017 Water-triggered ductile-brittle transition of anisotropic lamellar hydrogels and effect of confinement on polymer dynamics *Macromolecules* **50** 8169-77

[27] Sun T L, Kurokawa T, Kuroda S, Ihsan A B, Akasaki T, Sato K, Haque Md. A, Nakajima T and Gong J P 2013 Physical hydrogels composed of polyampholytes demonstrate high toughness and viscoelasticity *Nat. Mater.* **17** 932-7

[28] Luo F , Sun T L, Nakajima T , Kurokawa T , Zhao Y , Sato K, Ihsan A B , Li X, Guo H and Gong J P 2015 Oppositely charged polyelectrolytes form tough, self-healing, and rebuildable hydrogels *Adv. Mater.* **27** 2722–7

[29] Luo F , Sun T L, Nakajima T, Kurokawa T, Zhao Y, Ihsan A B, Guo H L, Li X F and Gong J P 2014 Crack blunting and advancing behaviors of tough and self-healing polyampholyte hydrogel *Macromolecules* **47** 6037−46

[30] Sun T L, Luo F, Hong W, Cui K, Huang Y, Zhang H J, King D R, Kurokawa T, Nakajima T and Gong J P 2017 Bulk energy dissipation mechanism for the fracture of tough and self-healing hydrogels *Macromolecules* **50** 2923−31

[31] Gao H, Wang N, Hu X, Nan W, Han Y and Liu W 2012 Double hydrogen-bonding pH-Sensitive hydrogels retaining high-strengths over a wide pH range *Macromol. Rapid Commun.* **34** 63-8

[32] Matsuda T, Kawakami R, Namba R, Nakajima T and Gong J P 2019 Mechanoresponsive self-growing hydrogels inspired by muscle training, *Science* **363** 504-8

[33] Lu H B, Xing Z Y, Hossain M and Fu Y Q 2019 Modeling strategy for dynamic-modal mechanophore in double-network hydrogel composites with self-growing and tailorable mechanical strength *Compo. Part B* **179** 107528

[34] Xing Z Y, Lu H B, Hossain M, Fu Y Q, Leng J S and Du S Y 2020 Cooperative dynamics of heuristic swelling and inhibitive micellization in double-network hydrogels by ionic dissociation of polyelectrolyte *Polymer* **186** 122039

[35] Cai W H, Lu S, Wei J H and Cui S X 2019 Single-chain polymer models incorporating the effects of side groups: An approach to general polymer models *Macromolecules* **52** 7324−30

[36] Flory P J and Volkenstein M 1969 *Statistical mechanics of chain molecules* (Wiley Online Library)

[37] Schuler B, Soranno A, Hofmann H and Nettels D 2016 Single-molecule FRET spectroscopy and the polymer physics of unfolded and intrinsically disordered proteins *Annu. Rev. Biophys.* **45** 207-31

[38] Flory P J 1953 *Principles of polymer chemistry* (New York: Cornell University Press)

[39] Treloar L R G 1975 *The physics of rubber elasticity* (New York: Oxford University Press)

[40] Gennes P G 1979 *Scaling concepts in polymer physics* (Ithaca and London :Cornell University Press)

[41] Xiang Y H, Zhong D M, Wang P, Yin T H, Zhou H F, Yu H H, Baliga C, Qu S X and Yang W 2019 A physically based visco-hyperelastic constitutive model for soft materials *J. Mech. Phys. Solids* **128** 208-18

[42] Xiang Y H, Zhong D M , Wang P, Mao G Y, Yu H H and Qu S X 2018 A general constitutive model of soft elastomers *J. Mech. Phys. Solids* **117** 110-22

[43] Kröger M 2015 Simple, admissible, and accurate approximants of the inverse Langevin and Brillouin functions, relevant for strong polymer deformations and flows *J. Non-Newton. Fluid* **223** 77-87

[44] Kuhl E, Menzel A and Garikipati K 2006 On the convexity of transversely isotropic chain network models *Philos. Mag.* **86** 3241-58

[45] Boyce M C and Arruda E M 2020 Constitutive Models of Rubber Elasticity: A Review *Rubber Chem. Technol.* **73** 504-23

[46] Hossain M and Steinmann P 2013 More hyperelastic models for rubber-like materials: consistent tangent operators and comparative study *J. Mech. Behav. Mater.* **22** 27-50

[47] Hossain M, Amin A F M S and Kabir M N 2015 Eight-chain and full-network models and their modified versions for rubber hyperelasticity: a comparative study *J. Mech. Behav. Mater.* **24** 11-24

[48] Zhao Y, Guan J and Wu S J 2019 Highly stretchable and tough physical silk fibroin-based double network hydrogels *Macromol. Rapid Commun.* **40** 1900389